

Training Deep Spiking Neural Networks using Backpropagation

Jun Haeng Lee^{*†}, Tobi Delbruck[†], Michael Pfeiffer[†]

^{*}Samsung Advanced Institute of Technology, Samsung Electronics
junhaeng2.lee@samsung.com

[†]Institute of Neuroinformatics, University of Zurich and ETH Zurich
{tobi, pfeiffer}@ini.uzh.ch

Abstract

Deep spiking neural networks (SNNs) hold great potential for improving the latency and energy efficiency of deep neural networks through event-based computation. However, training such networks is difficult due to the non-differentiable nature of asynchronous spike events. In this paper, we introduce a novel technique, which treats the membrane potentials of spiking neurons as differentiable signals, where discontinuities at spike times are only considered as noise. This enables an error backpropagation mechanism for deep SNNs, which works directly on spike signals and membrane potentials. Thus, compared with previous methods relying on indirect training and conversion, our technique has the potential to capture the statics of spikes more precisely. Our novel framework outperforms all previously reported results for SNNs on the permutation invariant MNIST benchmark, as well as the N-MNIST benchmark recorded with event-based vision sensors.

1 Introduction

Deep learning is achieving outstanding results in various machine learning tasks [9, 14], but for applications that require real-time interaction with the real environment, the repeated and often redundant update of large numbers of units becomes a bottleneck for efficiency. An alternative has been proposed in the form of spiking neural networks (SNNs), a major research topic in theoretical neuroscience and neuromorphic engineering. SNNs exploit event-based, data-driven updates to gain efficiency, especially if they are combined with inputs from event-based sensors, which reduce redundant information based on asynchronous event processing [2, 19, 22]. Even though in theory [17] SNNs have been shown to be as computationally powerful as conventional artificial neural networks (ANNs, this term will be used to describe conventional deep neural networks in contrast with SNNs), practically SNNs have not quite reached the same accuracy levels of ANNs in traditional machine learning tasks. A major reason for this is the lack of adequate training algorithms for deep SNNs, since spike signals are not differentiable, but differentiable activation functions are fundamental for using error backpropagation. A recently proposed solution is to use different data representations between training and processing, i.e. training a conventional ANN and developing conversion algorithms that transfer the weights into equivalent deep SNNs [4, 5, 11, 22]. However, in these methods, details of statistics in spike trains that go beyond mean rates, such as required for processing event-based sensor data cannot be precisely represented by the signals used for training. It is therefore desirable to devise learning rules operating directly on spike trains, but so far it has only been possible to train single layers, and use unsupervised learning rules, which leads to a deterioration of accuracy [3, 18, 20]. An alternative approach has recently been introduced by [23], in which a SNN learns from spikes, but requires keeping statistics for computing stochastic gradient descent (SGD) updates in order to approximate a conventional ANN. In this paper we introduce a novel supervised learning technique, which can train general forms of deep SNNs directly from

spike signals. This includes SNNs with leaky membrane potential and spiking winner-takes-all (WTA) circuits. The key idea of our approach is to generate a continuous and differentiable signal on which SGD can work, using low-pass filtered spiking signals added onto the membrane potential and treating abrupt changes of the membrane potential as noise during error backpropagation. Additional techniques are presented that address particular challenges of SNN training: spiking neurons typically require large thresholds to achieve stability and reasonable firing rates, but this may result in many “dead” neurons, which do not participate in the optimization during training. Novel regularization and normalization techniques are presented, which contribute to stable and balanced learning. Our techniques lay the foundations for closing the performance gap between SNNs and ANNs, and promote their use for practical applications.

2 Related Work

Gradient descent methods for SNNs have not been deeply investigated because of the non-differentiable nature of spikes. The most successful approaches to date have used indirect methods, such as training a network in the continuous rate domain and converting it into a spiking version. O’Connor et al. pioneered this area by training a spiking deep belief network (DBN) based on the Siebert event-rate approximation model [22], but only reached accuracies around 94.09% for the MNIST hand written digit classification task. Hunsberger and Eliasmith used the softened rate model for leaky integrate and fire (LIF) neurons [11], training an ANN with the rate model and converting it into a SNN consisting of LIF neurons. With the help of pre-training based on denoising autoencoders they achieved 98.6% in the permutation-invariant (PI) MNIST task. Diehl et al. [4] trained deep neural networks with conventional deep learning techniques and additional constraints necessary for conversion to SNNs. After the training units were converted into spiking neurons and the performance was optimized by normalization of weight parameters, yielding 98.64% accuracy in the PI MNIST task. Esser et al. [5] used a differentiable probabilistic spiking neuron model for training and statistically sampled the trained network for deployment. In all of these methods, training was performed indirectly using continuous signals, which may not capture important statistics of spikes generated by sensors used during processing time. Even though SNNs are optimally suited for processing signals from event-based sensors such as the Dynamic Vision Sensor (DVS) [16], the previous SNN training models require to get rid of time information and generate image frames from the event streams. Instead, we use the same signal format for training and processing deep SNNs, and can thus train SNNs directly on spatio-temporal event streams. This is demonstrated on the neuromorphic N-MNIST benchmark dataset [24], outperforming all previous attempts that ignored spike timing.

3 Spiking Neural Networks

In this article we study fully connected SNNs with multiple hidden layers. Let M and N be the number of synapses of a neuron and the number of neurons in a layer, respectively. On the other hand, m and n are the number of active synapses (i.e. synapses receiving spike inputs) of a neuron and the number of active neurons (sending spike outputs) in a layer. We will also use the simplified form of indices for active synapses and neurons throughout the paper as

$$\text{Active synapses: } \{v_1, \dots, v_m\} \rightarrow \{1, \dots, m\}, \text{ Active neurons: } \{u_1, \dots, u_n\} \rightarrow \{1, \dots, n\}$$

Thus, if an index i , j , or k is used for a synapse over $[1, m]$ or a neuron over $[1, n]$ (e.g. in (4)), it actually represents an index of an active synapse (v_i) or an active neuron (u_j).

3.1 Leaky Integrate-and-Fire (LIF) Neuron

The LIF neuron is one of the simplest models used for describing dynamics of spiking neurons [6]. Since the states of LIF neurons can be updated asynchronously based on the timing of input events, it is a very efficient model in terms of computational cost. For a given input spike the membrane potential of a LIF neuron can be updated as

$$V_{mp}(t_p) = V_{mp}(t_{p-1})e^{-\frac{t_p - t_{p-1}}{\tau_{mp}}} + w_i^{(p)}w_{dyn}, \quad (1)$$

where V_{mp} is the membrane potential, τ_{mp} is the membrane time constant, t_p and t_{p-1} are the present and previous input spike times, $w_i^{(p)}$ is the synaptic weight of the i -th synapse (through which the present p -th input spike arrives). w_{dyn} is a dynamic weight controlling the refractory period, defined as $w_{dyn} = w_{d0} + (\Delta_t/T_{ref})^2$ if $\Delta_t < T_{ref}$ and $w_{dyn} < 1$, and $w_{dyn} = 1$ otherwise. T_{ref} is the refractory period, w_{d0} is the initial value (usually 0), and $\Delta_t = t_{out} - t_p$, where t_{out} is the time of the latest output spike produced by the neuron. Thus, the effect of input spikes on V_{mp} is suppressed for a short period of time T_{ref} after an output spike. w_{dyn} recovers quadratically to 1 after the output spike at t_{out} . Since w_{dyn} is applied to all synapses identically, it is different from short-term plasticity, which is a synapse specific mechanism. When V_{mp} crosses the threshold value V_{th} , the LIF neuron generates an output spike and V_{mp} is decreased by a fixed amount proportional to the threshold:

$$V_{mp}(t_p^+) = V_{mp}(t_p) - \gamma V_{th}, \quad (2)$$

where γ is the membrane potential reset factor and t_p^+ is time right after the reset. We used $\gamma = 1$ for all the results in this paper. The valid range of the membrane potential is limited to $[-V_{th}, V_{th}]$. Since the upper limit is guaranteed by (2), the membrane potential is clipped to $-V_{th}$ when it falls below this value. This strategy helps balancing the participation of neurons during training. We will revisit this issue when we introduce threshold regularization in Section 5.2.

3.2 Winner-Take-All (WTA) Circuit

We found that the accuracy of SNNs could be improved by introducing a competitive recurrent architecture called WTA circuit in certain layers. In a WTA circuit, multiple neurons form a group with lateral inhibitory connections. Thus, as soon as any neuron produces an output spike, it inhibits all other neurons in the circuit and prevents them from spiking [25]. In this work, all lateral connections in a WTA circuit have the same strength, which reduces memory and computational costs for implementing them. The amount of lateral inhibition applied to the membrane potential is designed to be proportional to the inhibited neuron’s membrane potential threshold (see (4) in Section 4.1). With this scheme, lateral connections inhibit neurons having small V_{th} weakly and those having large V_{th} strongly. This improves the balance of activities among neurons during training. As shown in Results, WTA competition in the SNN led to remarkable improvements, especially in networks with a single hidden layer. The WTA circuit also improves the stability and speed of training.

4 Using Backpropagation in SNNs

We now derive the transfer function for spiking neurons in WTA configuration and the SNN backpropagation equations. We also introduce simple methods to initialize parameters and normalize backpropagating errors to address vanishing or exploding gradients, and to stabilize training.

4.1 Transfer function and derivatives

From the event-based update in (1), the accumulated effects of the k -th synapse onto the membrane potential (normalized by synaptic weight) and the membrane potential reset in (2) (normalized by γV_{th}) at time t can be derived as

$$x_k(t) = \sum_p \exp\left(\frac{t_p - t}{\tau_{mp}}\right), \quad a_i(t) = \sum_q \exp\left(\frac{t_q - t}{\tau_{mp}}\right), \quad (3)$$

where the sum is over all input spike times $t_p < t$ of the synapse for x_k , and the output spike times $t_q < t$ for a_i . The accumulated effects of lateral inhibitory signals in WTA circuits can be expressed analogously to (3). Ignoring the effect of refractory periods for now, this means that the membrane potential of the i -th active neuron in a WTA circuit can be written as

$$V_{mp,i}(t) = \sum_{k=1}^m w_{ik} x_k(t) - \gamma V_{th,i} a_i(t) + \sigma V_{th,i} \sum_{j=1, j \neq i}^n \kappa_{ij} a_j(t). \quad (4)$$

The terms on the right side represent the input, membrane potential resets, and lateral inhibition, respectively. x_k denotes the effect of the k -th active input neuron, and a_i the effect induced by output activity of the i -th active neuron, as defined in (3). κ_{ij} is the strength of lateral inhibition ($-1 \leq \kappa_{ij} < 0$) from the j -th active neuron to the i -th active neuron, and σ is the expected efficacy of lateral inhibition. σ should be smaller than 1, since lateral inhibitions can affect the membrane potential only down to its lower bound (i.e. $-V_{th}$). We found a value of $\sigma \approx 0.5$ to work well in practice. Eq. (4) reveals the relationship between inputs and outputs of spiking neurons which is not clearly shown in (1) and (2). Since the output (a_i) of the current layer becomes the input (x_k) of the next layer if all the neurons have same τ_{mp} , (4) provides the basis for backpropagation. Differentiation is not defined in (3) at the moment of each spike because of a step jump. However, we can regard these jumps as noise while treating (3) and (4) as differentiable continuous signals to derive derivatives for backpropagation. In previous works [4, 5, 11, 22], continuous variables were introduced as a surrogate for x_k and a_i in (4) for backpropagation. In this work, however, we directly use the contribution of spike signals to the membrane potential as defined in (3). Thus, the real statistics of spike signals, including temporal effects such as synchrony between inputs, can influence the training process. Ignoring the step jumps caused by spikes in the calculation of gradients might of course introduce errors, but we found in practice that this has very little influence on SNN training. A potential explanation is that by regarding the signals in (3) as continuous signals, but corrupted by noise at the times of spikes, this can have a similar positive effect as the widely used approach of noise injection during training, which can improve the generalization capability of neural networks [28]. In the case of SNNs, several papers have used the trick of treating spike-induced abrupt changes as noise for gradient descent optimization [1, 11]. However, in these cases the model added Gaussian random noise instead of spike-induced perturbations. In this work, we directly use the actual contribution of spike signals to the membrane potential as described in (3) for training SNNs. Here we show that this approach works well for learning in SNNs where information is encoded in spike rates, but importantly, the presented framework also provides the basis for utilizing specific spatio-temporal codes, which we demonstrate on a task using directly inputs from event-based sensors.

For the backpropagation equations we need to obtain the transfer functions of LIF neurons in the WTA circuit. For this we set the residual V_{mp} term in the left side of (4) to zero (since it is not relevant to the transfer function), resulting in the transfer function

$$a_i \approx \frac{s_i}{\gamma V_{th,i}} + \frac{\sigma \sum_{j=1, j \neq i}^n \kappa_{ij} a_j}{\gamma}, \text{ where } s_i = \sum_{k=1}^m w_{ik} x_k. \quad (5)$$

Refractory periods are not considered here since the activity of neurons in SNNs is rarely dominated by refractory periods in a normal operating regime. For example, we used a refractory period of 1 ms and the event rates of individual neurons were kept within a few tens of events per second (eps). Eq. (5) is consistent with (4.9) in [6] without WTA terms. It can also be simplified to a spiking version of a rectified-linear unit by introducing a unit threshold and non-leaky membrane potential as in [23]. Directly differentiating (5) yields the backpropagation equations

$$\frac{\partial a_i}{\partial s_i} \approx \frac{1}{\gamma V_{th,i}}, \frac{\partial a_i}{\partial w_{ik}} \approx \frac{\partial a_i}{\partial s_i} x_k, \frac{\partial a_i}{\partial V_{th,i}} \approx \frac{\partial a_i}{\partial s_i} (-\gamma a_i + \sigma \sum_{j \neq i}^n \kappa_{ij} a_j), \frac{\partial a_i}{\partial \kappa_{ih}} \approx \frac{\partial a_i}{\partial s_i} (\sigma V_{th,i} a_h), \quad (6)$$

$$\begin{bmatrix} \frac{\partial a_1}{\partial x_k} \\ \vdots \\ \frac{\partial a_1}{\partial x_k} \end{bmatrix} \approx \frac{1}{\sigma} \begin{bmatrix} q & \cdots & -\kappa_{1n} \\ \vdots & \ddots & \vdots \\ -\kappa_{n1} & \cdots & q \end{bmatrix}^{-1} \begin{bmatrix} \frac{w_{1k}}{V_{th,1}} \\ \vdots \\ \frac{w_{nk}}{V_{th,n}} \end{bmatrix} \quad (7)$$

where $q = \gamma/\sigma$. When all the lateral inhibitory connections have the same strength ($\kappa_{ij} = \mu, \forall i, j$) and are not learned, $\partial a_i / \partial \kappa_{ih}$ is not necessary and (7) can be simplified to

$$\frac{\partial a_i}{\partial x_k} \approx \frac{\partial a_i}{\partial s_i} \frac{\gamma}{(\gamma - \mu\sigma)} \left(w_{ik} - \frac{\mu\sigma V_{th,i}}{\gamma + \mu\sigma(n-1)} \sum_{j=1}^n \frac{w_{jk}}{V_{th,j}} \right). \quad (8)$$

We consider only the first-order effect of the lateral connections in the derivation of gradients. Higher-order terms propagating back through multiple lateral connections are neglected for simplicity. This is mainly

because all the lateral connections considered here are inhibitory. For inhibitory lateral connections, the effect of small parameter changes decays rapidly with connection distance. Thus, first-order approximation saves a lot of computational cost without loss of accuracy.

4.2 Initialization and Error Normalization

Good initialization of weight parameters in supervised learning is critical to handle the exploding or vanishing gradients problem in deep neural networks [7, 10]. The basic idea behind those methods is to maintain the balance of forward activations and backward propagating errors among layers. Recently, the batch normalization technique has been proposed to make sure that such balance is maintained through the whole training process [12]. However, normalization of activities as in the batch normalization scheme is difficult for SNNs, because there is no efficient method for amplifying event rates. The initialization methods proposed in [7, 10] are not appropriate for SNNs either, because SNNs have positive thresholds that are usually much larger than individual weight values. In this work, we propose simple methods for initializing parameters and normalizing backprop errors for training deep SNNs. Even though the proposed technique does not guarantee the balance of forward activations, it is effective for addressing the exploding and vanishing gradients problems. The weight and threshold parameters of neurons in the l -th layer are initialized as

$$w^{(l)} \sim U \left[-\sqrt{3/M^{(l)}}, \sqrt{3/M^{(l)}} \right], \quad V_{th}^{(l)} = \alpha \sqrt{3/M^{(l)}}, \quad \alpha > 1, \quad (9)$$

where $U[-a, a]$ is the uniform distribution in the interval $(-a, a)$, $M^{(l)}$ is the number of synapses of each neuron, and α is a constant. α should be large enough to stabilize spiking neurons, but small enough to make the neurons respond to the inputs through multiple layers. We used values between 3 and 10 for α . The weights initialized by (9) satisfy the following condition:

$$E \left[\sum_i^{M^{(l)}} (w_{ji}^{(l)})^2 \right] = 1 \quad \text{or} \quad E \left[(w_{ji}^{(l)})^2 \right] = \frac{1}{M^{(l)}}. \quad (10)$$

This condition is used for backprop error normalization in the next paragraph. In addition, to ensure stability, the weight parameters are regularized by decaying them so that they do not deviate too much from (10) throughout training. We will discuss this in detail in Section 5.1.

The main idea of backprop error normalization is to balance the magnitude of updates in weights (and in threshold) parameters among layers. In the l -th layer ($N^{(l)} = M^{(l+1)}$, $n^{(l)} = m^{(l+1)}$), we define the error propagating back through the i -th active neuron as

$$\delta_i^{(l)} = \frac{g_i^{(l)}}{\bar{g}^{(l)}} \sqrt{\frac{M^{(l+1)}}{m^{(l+1)}}} \sum_j^{n^{(l+1)}} w_{ji}^{(l+1)} \delta_j^{(l+1)}, \quad (11)$$

where $g_i^{(l)} = 1/V_{th,i}^{(l)}$, $\bar{g}^{(l)} = \sqrt{E \left[(g_i^{(l)})^2 \right]} \cong \sqrt{\frac{1}{n^{(l)}} \sum_i^{n^{(l)}} (g_i^{(l)})^2}$. Thus, with (10), the expectation of the squared sum of errors (i.e., $E[\sum_i^{n^{(l)}} (\delta_i^{(l)})^2]$) can be maintained constant through layers. Although this was confirmed for the case without a WTA circuit, we found that it still approximately holds for networks using WTA. Weight and threshold parameters are updated as:

$$\Delta w_{ij}^{(l)} = -\eta_w \sqrt{\frac{N^{(l)}}{m^{(l)}}} \delta_i^{(l)} \hat{x}_j^{(l)}, \quad \Delta V_{th,i}^{(l)} = -\eta_{th} \sqrt{\frac{N^{(l)}}{m^{(l)} M^{(l)}}} \delta_i^{(l)} \hat{a}_i^{(l)}, \quad (12)$$

where η_w and η_{th} are the learning rates for weight and threshold parameters, respectively. We found that the threshold values tend to decrease through the training epochs due to SGD decreasing the threshold values whenever the target neuron does not fully respond to the corresponding input. Small thresholds, however, could lead to exploding firing within the network. Thus, we used smaller learning rates for threshold updates to prevent the threshold parameters from decreasing too much. \hat{x} and \hat{a} in (12) are the effective input and output activities defined as: $\hat{x}_j = x_j$, $\hat{a}_i = \gamma a_i - \sigma \sum_{j \neq i}^n \kappa_{ij} a_j$. By using (12), at the initial stage of training, the amount of updates depends on the expectation of per-synapse activity of active inputs, regardless of the number of active synapses or neurons. Thus, we can balance updates among layers in deep SNNs.

5 Regularization

As in conventional ANNs, regularization techniques such as weight decay during training are essential to improve the generalization capability of SNNs. Another problem in training SNNs is that because thresholds need to be initialized to large values, only a few neurons respond to input stimuli and many of them remain silent. This is a significant problem, especially in WTA circuits. In this section we introduce weight and threshold regularization methods to address these problems.

5.1 Weight Regularization

Weight decay regularization is used to improve the stability of SNNs as well as their generalization capability. Specifically, we want to maintain the condition in (10). Conventional L2-regularization was found to be inadequate for this purpose, because it leads to an initial fast growth, followed by a continued decrease of weights. To address this issue, a new method named exponential regularization is introduced, which is inspired from max-norm regularization [27]. The cost function of exponential regularization for neuron i of layer l is defined as:

$$L_w(l, i) = \frac{1}{2} \lambda e^{\beta \left(\sum_j^{M^{(l)}} (w_{ij}^{(l)})^2 - 1 \right)}, \quad (13)$$

where β and λ are parameters to control the balance between error correction and regularization. L2-regularization has a constant rate of decay regardless of weight values, whereas max-norm regularization imposes an upper bound of weight increase. Exponential regularization is a compromise between the two. The decay rate is exponentially proportional to the squared sum of weights. Thus, it strongly prohibits the increase of weights like max-norm regularization. Weight parameters are always decaying in any range of values to improve the generalization capability as in L2-regularization. However, exponential regularization prevents weights from decreasing too much by reducing the decay rate. Thus, the magnitude of weights can be easily maintained at a certain level.

5.2 Threshold Regularization

Threshold regularization is used to balance the activities among N neurons receiving the same input stimuli. When N_w neurons fire after receiving an input spike, their thresholds are increased by ρN_w . Subsequently, for all N neurons, the threshold is decreased by ρN_w . Thus, highly active neurons become less sensitive to input stimuli due to the increase of their thresholds. On the other hand, rarely active neurons can respond more easily for subsequent stimuli. Because the membrane potentials are restricted to the range $[-V_{th}, V_{th}]$, neurons with smaller thresholds, because of their tight lower bound, tend to be less influenced by negative inputs. Threshold regularization actively prevents dead neurons and encourages all neurons to equally contribute to the optimization. This kind of regularization has been used for competitive learning previously [26]. We set a lower bound on thresholds to prevent spiking neurons from firing too much due to extremely small threshold values. If the threshold of a neuron is supposed to go below the lower bound, then instead of decreasing the threshold, all weight values of the neuron are increased by the same amount. Threshold regularization was done during the forward propagation in training.

6 Results and Discussion

Using the regularization term from (13), the objective function for each training sample (using batch size = 1) is given by $L = \frac{1}{2} \|a - y\|^2 + \sum_{l \in \text{hidden}} \sum_i L_w(l, i)$, where y is the label vector and a is the output vector. Each element of a is defined as $a_i = \#spike_i / \max_j(\#spike_j)$, where $\#spike_i$ is the number of output spikes generated by the i -th neuron of the output layer. The output is normalized by the maximum value instead of the sum of all outputs. With this scheme, it is not necessary to use weight regularization for the output layer.

The PI MNIST task was used for performance evaluation [15]. MNIST is a hand written digit classification dataset consisting of 60,000 training samples and 10,000 test samples. The permutation-invariant version was chosen to directly measure the power of the fully-connected classifier. By randomly permuting the input stimuli

Table 1: Values of parameters used in the experiments

| Parameters | Values | Used In |
|-------------|------------------------------------|----------|
| τ_{mp} | 20 ms (MNIST), 200 ms (N-MNIST) | (1), (3) |
| T_{ref} | 1 ms | (1) |
| α | 3 – 10 | (9) |
| η_w | 0.002 – 0.004 | (12) |
| η_{th} | $0.1\eta_w$ (SGD), η_w (ADAM) | (12) |
| β | 10 | (13) |
| λ | 0.002 – 0.04 | (13) |
| ρ | 0.00004 – 0.0002 | 5.2 |

we prohibit the use of techniques that exploit spatial correlations within inputs, such as data augmentation or convolutions to improve performance. An event stream is generated from a 28×28 pixel image of a hand written digit at the input layer. The intensity of each pixel defines the event rate of Poisson events. We normalized the total event rate to be 5 keps (~ 43 eps per non-zero pixel on average). The accuracy of the SNN tends to improve as the integration time (i.e. the duration of the input stimuli) increases. We used 1 second duration of the input event stream during accuracy measurements to obtain stable results. Further increase of integration time improved the accuracy only marginally ($< 0.1\%$). During training, only 50 ms presentations per digit were used to reduce the training time. In the initial phase of training deep SNNs, neuron activities tend to quickly decrease propagating into higher layers due to non-optimal weights and large thresholds. Thus, for the networks with 2 hidden layers (HLs), the first epoch was used as an initial training phase by increasing the duration of the input stimuli to 200 ms. All 60,000 samples were used for training, and 10,000 samples for testing. No validation set or early stopping were used. Learning rate and threshold regularization were decayed by $\exp(-1/35)$ every epoch. Typical values for parameters are listed in Table 1. We trained and evaluated SNNs with different sized hidden layers (784- N -10, where $N = 100, 200, 300$) and varied the strength of lateral inhibitory connections in WTA circuits (in the HL and the output layer) to find their optimum value. All the networks were initialized with the same weight values and trained for 150 epochs. The reported accuracy is the average over epochs [131, 150], which reduces the fluctuation caused by random spike timing in the input spike stream and training. Figure 1(a) shows the accuracy measured by varying the lateral inhibition strength in the first HL. The best performance was obtained when the lateral inhibition was at -0.4, regardless of N . For the output layer, we found that -1.0 gave the best result. Table 2 show the accuracies of various shallow and deep architectures in comparison with previous reports. For the deep SNNs with 2 HLs, the first HL and the output layer were competing in a WTA circuit. The strength of the lateral inhibition was -0.4 and -1.0 for each one as in the case of the SNNs with 1 HL. However, for the second HL, the best accuracy was obtained without a WTA circuit, which possibly means that the outputs of the first hidden layer cannot be sparsified as much as the original inputs without losing information. The best accuracy (98.64%) obtained from the SNN with 1 HL was better than that of the shallow ANN (i.e. MLP) (98.4%) and matched the previous state-of-the-art of deep SNNs [4, 11]. We attribute this improvement to the use of WTA circuits and the direct optimization on spike signals. The best accuracy of SNN with 2 HLs was 98.7% with vanilla SGD. By applying the ADAM learning method ($\beta_1 = 0.9, \beta_2 = 0.999, \epsilon = 10^{-8}$) [13], we could further improve the best accuracy up to 98.77%, which is in the range of ANNs trained with Dropout or DropConnect [27, 29].

To investigate the potential of the proposed method on event stream data, we trained simple networks with 1 HL on the N-MNIST dataset, a neuromorphic version of MNIST. It was generated by moving a Dynamic Vision Sensor (DVS) [16] in front of projected images of digits [24]. A 3-phase saccadic movement of the DVS (Figure 1(b)) is responsible for generating events, and shifts the position of the digit in pixel space. The previous state-of-the-art result achieved 95.72% accuracy with a spiking convolutional neural network (CNN) [21]. Their approach was based on [4], converting an ANN to an SNN instead of directly training on spike trains. This led to a large accuracy drop after conversion (98.3% \rightarrow 95.72%), even though the event streams were pre-processed to center the digits. In this work, however, we work directly on the original uncentered data. For training, 300 consecutive events were picked at random positions from each event stream, whereas the full event streams were used for evaluating the test accuracy. Since the DVS generated two types of event

Table 2: Comparison of accuracy of different models on PI MNIST without unsupervised pre-training or cost function (except SNN([22]) and SNN([11])) and N-MNIST [24].

| Network | # units in HLs | Test accuracy (%) |
|---------------------------------------|---------------------------------|------------------------|
| ANN ([27], Drop-out) | 4096-4096 | 98.99 |
| ANN ([29], Drop-connect) | 800-800 | 98.8 |
| ANN ([8], maxout) | 240×5 - 240×5 | 99.06 |
| SNN ([22]) ^{a,b} | 500-500 | 94.09 |
| SNN ([11]) ^a | 500-300 | 98.6 |
| SNN ([4]) | 1200-1200 | 98.64 |
| SNN ([23]) | 200-200 | 97.8 |
| SNN (SGD, This work) | 800 | [98.56, 98.64, 98.71]* |
| SNN (SGD, This work) | 500-500 | [98.63, 98.70, 98.76]* |
| SNN (ADAM, This work) | 300-300 | [98.71, 98.77, 98.88]* |
| N-MNIST (centered), ANN ([21]) | CNN | 98.3 |
| N-MNIST (centered), SNN ([21]) | CNN | 95.72 |
| N-MNIST (uncentered), SNN (This work) | 500 | [98.45, 98.53, 98.61]* |

a: pretraining, b: data augmentation, *:[min, average, max] values over epochs [181, 200].

(on-event for intensity increase, off-event for intensity decrease), we separated events into two channels based on the event type. Table 2 shows that our result of 98.53% with 500 hidden units is the best N-MNIST result with SNNs reported to date.

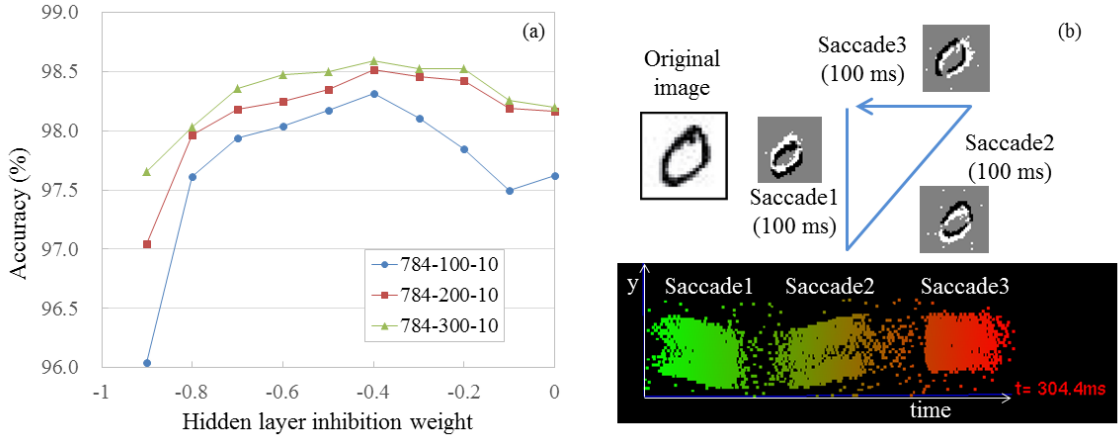


Figure 1: (a) Accuracy vs. strength of lateral inhibition in the hidden layer for PI MNIST. (b) Illustration of the saccades used to generate the N-MNIST dataset and resulting event streams [24].

We have shown that our novel spike-based backpropagation technique for deep SNNs works both on standard benchmarks such as PI MNIST, but also on N-MNIST, which contains rich spatio-temporal structure in the events generated by a neuromorphic vision sensor. We improve the previous state-of-the-art of SNNs on both tasks and achieve accuracy levels that match those of conventional deep networks. Closing this gap makes deep SNNs attractive for tasks with highly redundant information or energy constrained applications, due to the benefits of event-based computation, and advantages of efficient neuromorphic processors [19]. We expect that the proposed technique can precisely capture the statistics of spike signals generated from event-based sensors, which is an important advantage over previous SNN training methods. Future work will extend our training approach to new architectures, such as CNNs and recurrent networks.

References

- [1] Y. Bengio, T. Mesnard, A. Fischer, S. Zhang, and Y. Wu. An objective function for stdp. *arXiv preprint arXiv:1509.05936*, 2015.
- [2] L. Camunas-Mesa, C. Zamarreño-Ramos, A. Linares-Barranco, A. J. Acosta-Jiménez, T. Serrano-Gotarredona, and B. Linares-Barranco. An event-driven multi-kernel convolution processor module for event-driven vision sensors. *IEEE Journal of Solid-State Circuits*, 47(2):504–517, 2012.
- [3] P. U. Diehl and M. Cook. Unsupervised learning of digit recognition using spike-timing-dependent plasticity. *Frontiers in Computational Neuroscience*, 9:99, 2015.
- [4] P. U. Diehl, D. Neil, J. Binas, M. Cook, S.-C. Liu, and M. Pfeiffer. Fast-classifying, high-accuracy spiking deep networks through weight and threshold balancing. In *International Joint Conference on Neural Networks (IJCNN)*, pages 1–8, 2015.
- [5] S. K. Esser, R. Appuswamy, P. Merolla, J. V. Arthur, and D. S. Modha. Backpropagation for energy-efficient neuromorphic computing. In *Advances in Neural Information Processing Systems*, pages 1117–1125, 2015.
- [6] W. Gerstner and W. M. Kistler. *Spiking neuron models: Single neurons, populations, plasticity*. Cambridge University Press, 2002.
- [7] X. Glorot and Y. Bengio. Understanding the difficulty of training deep feedforward neural networks. In *International conference on artificial intelligence and statistics*, pages 249–256, 2010.
- [8] I. J. Goodfellow, D. Warde-Farley, M. Mirza, A. Courville, and Y. Bengio. Maxout networks. *arXiv preprint arXiv:1302.4389*, 2013.
- [9] K. He, X. Zhang, S. Ren, and J. Sun. Deep residual learning for image recognition. *arXiv preprint arXiv:1512.03385*, 2015.
- [10] K. He, X. Zhang, S. Ren, and J. Sun. Delving deep into rectifiers: Surpassing human-level performance on imagenet classification. In *Proceedings of the IEEE International Conference on Computer Vision*, pages 1026–1034, 2015.
- [11] E. Hunsberger and C. Eliasmith. Spiking deep networks with lif neurons. *arXiv preprint arXiv:1510.08829*, 2015.
- [12] S. Ioffe and C. Szegedy. Batch normalization: Accelerating deep network training by reducing internal covariate shift. *arXiv preprint arXiv:1502.03167*, 2015.
- [13] D. Kingma and J. Ba. Adam: A method for stochastic optimization. *arXiv preprint arXiv:1412.6980*, 2014.
- [14] Y. LeCun, Y. Bengio, and G. Hinton. Deep learning. *Nature*, 521(7553):436–444, 2015.
- [15] Y. LeCun, L. Bottou, Y. Bengio, and P. Haffner. Gradient-based learning applied to document recognition. *Proceedings of the IEEE*, 86(11):2278–2324, 1998.
- [16] P. Lichtsteiner, C. Posch, and T. Delbruck. A 128×128 120 db 15 μ s latency asynchronous temporal contrast vision sensor. *IEEE Journal of Solid-State Circuits*, 43(2):566–576, 2008.
- [17] W. Maass and H. Markram. On the computational power of circuits of spiking neurons. *Journal of computer and system sciences*, 69(4):593–616, 2004.
- [18] T. Masquelier and S. J. Thorpe. Unsupervised learning of visual features through spike timing dependent plasticity. *PLoS Computational Biology*, 3(2):e31, 2007.
- [19] P. A. Merolla, J. V. Arthur, R. Alvarez-Icaza, A. S. Cassidy, J. Sawada, F. Akopyan, B. L. Jackson, N. Imam, C. Guo, Y. Nakamura, et al. A million spiking-neuron integrated circuit with a scalable communication network and interface. *Science*, 345(6197):668–673, 2014.
- [20] E. Nefci, S. Das, B. Pedroni, K. Kreutz-Delgado, and G. Cauwenberghs. Event-driven contrastive divergence for spiking neuromorphic systems. *Frontiers in Neuroscience*, 7:272, 2014.
- [21] D. Neil and S.-C. Liu. Effective sensor fusion with event-based sensors and deep network architectures. In *IEEE Int. Symposium on Circuits and Systems (ISCAS)*, 2016.

- [22] P. O'Connor, D. Neil, S.-C. Liu, T. Delbruck, and M. Pfeiffer. Real-time classification and sensor fusion with a spiking deep belief network. *Frontiers in Neuromorphic Engineering*, 7, 2013.
- [23] P. O'Connor and M. Welling. Deep spiking networks. *arXiv preprint arXiv:1602.08323*, 2016.
- [24] G. Orchard, A. Jayawant, G. K. Cohen, and N. Thakor. Converting static image datasets to spiking neuromorphic datasets using saccades. *Frontiers in Neuroscience*, 9, 2015.
- [25] C. J. Rozell, D. H. Johnson, R. G. Baraniuk, and B. A. Olshausen. Sparse coding via thresholding and local competition in neural circuits. *Neural Computation*, 20(10):2526–2563, 2008.
- [26] D. E. Rumelhart and D. Zipser. Feature discovery by competitive learning. *Cognitive science*, 9(1):75–112, 1985.
- [27] N. Srivastava, G. Hinton, A. Krizhevsky, I. Sutskever, and R. Salakhutdinov. Dropout: A simple way to prevent neural networks from overfitting. *Journal of Machine Learning Research*, 15(1):1929–1958, 2014.
- [28] P. Vincent, H. Larochelle, Y. Bengio, and P.-A. Manzagol. Extracting and composing robust features with denoising autoencoders. In *Proc. of the 25th International Conference on Machine learning*, pages 1096–1103, 2008.
- [29] L. Wan, M. Zeiler, S. Zhang, Y. L. Cun, and R. Fergus. Regularization of neural networks using dropconnect. In *Proceedings of the 30th International Conference on Machine Learning*, pages 1058–1066, 2013.